

A Molecular Dynamics Study of Lunasin

Parvesh Singh^a and Krishna Bisetty^{a,*}

^aDepartment of Chemistry, Durban University of Technology, Steve Biko campus, P.O. Box 1334, Durban, 4000, South Africa.

Received 18 November 2011, revised 13 March 2012, accepted 8 May 2012.

Submitted by invitation to celebrate 2011 the 'International Year of Chemistry'.

ABSTRACT

Lunasin, a 43 amino acid peptide, suppresses chemically induced transformations in mammalian cells and skin carcinogenesis in mice. This peptide has also been reported to exhibit very good bioavailability after its oral administration. However, despite its biological and medicinal significance, the exact three-dimensional (3D) structure of lunasin is thus far not yet fully characterized. Thus this work is aimed at exploring the conformational profile of lunasin, using classical molecular dynamics (MD) simulations at the time scale of 300 ns. The results obtained from the MD trajectory reveal that lunasin has a strong propensity to exhibit three characteristic α helical bundles in its structure supported by residues His⁵-Cys¹⁰, Cys²²-Ile³⁰ and Asp³⁵-Asp⁴¹. The reported cell adhesion motif (Arg-Gly-Asp) of lunasin responsible for its binding to cell chromatin, on other hand, did not exhibit any characteristic secondary feature. The structural information obtained from the current study could be useful to better understand the bioactive conformation of lunasin.

KEYWORDS

Lunasin, molecular dynamics, amber, CLASICO, α -helix, β -turn, PTRAJ, RGD, RMSD.

1. Introduction

Lunasin, a cancer-preventive peptide, was originally isolated from soybean cotyledon¹ and contains 43 amino acid residues with a cell adhesion motif composed of arginine-glycine-aspartic acid (RGD) residues² and a carboxylic acid tail of nine aspartic acid (AA) residues. The nine AA residues in the tail region are believed to be responsible for its direct binding with the chromatin and its antimitotic action in the mammalian cell lines. Reported biological activity of lunasin includes anti-inflammatory activity,³ inhibition of histone acetylation,⁴ reduction of skin tumour,⁵ inhibition of colony formation in NIH 3T3 cells treated with ras-oncogene,⁶ and slowing down of epidermal cell proliferation in mouse skin.⁷ The anti-inflammatory action of lunasin and other peptides in soybean is reportedly associated with the inhibition of pro-inflammatory markers including nuclear factor-kappa B (NF- κ B) transactivation, cyclooxygenase-2 expression, nitric oxide production, inducible nitric oxide synthase expression, prostaglandin E2 production, interleukin-6 production and interleukin-1 β production.⁸

Bioavailability studies conducted in both animals and humans revealed that approximately 35 % of ingested lunasin reaches the target tissues and organs in an intact and active form.⁹ The Bowman-Birk protease inhibitor (BBI) and Kunitztrypsin inhibitor (KTI) present in soybean are reported to be responsible for its protection against gastrointestinal tract digestion.¹⁰ The high cost involved in lunasin synthesis limits its applications to chemo-preventative and nutritional interventions, and thus prompts the search for new peptidomimetics with similar properties. The first step in this direction is to better understand the three dimensional (3D) structure of lunasin peptide, responsible for its biological actions.

A literature survey reveals that, despite having immense medicinal significance, there is a lack of experimental studies of the 3D structure of lunasin. The objective of the present study is therefore to gain a deeper understanding of the lunasin struc-

ture responsible for its biological actions by exploring the conformational profile of lunasin using standard MD simulations at the time scale of 300 ns using the AMBER 9 computer program.¹¹ Based on our previous studies performed on different peptides^{12–14}, the Generalized Born/surface area (GB/SA) procedure was employed, since it offers higher computational efficiency and reproduces accurately the results of explicit solvent simulations when used in combination with implicit solvent models with the AMBER ff 96 force field.^{15,16} Analysis of the MD trajectory was carried out using the CLASICO program¹⁷ and the PTRAJ module in AMBER 9.¹¹

2. Computational Methodology

The extended conformation of the 43 residue structural analogue [SKWQHQQDSCRKQKQGVNLTPEKHIMEKIQGRGDDDDDDDDDD] of the lunasin peptide was generated using the tleap module of AMBER 9,¹¹ and used as starting structures for the MD simulations. First, the peptide was energetically minimized using 1000 steps of steepest gradient, followed by a subsequent minimization using the conjugate gradient algorithm until a convergence of the gradient norm was lower than 0.005 kcal mol⁻¹ Å⁻¹. Following this the structures were equilibrated for 20 ps by gradually increasing the temperature from 0 to 300 K. MD trajectories were conducted using the generalized Born (GB) approximation at constant temperature (300 K) regulated by the Langevin algorithm as a thermostat.¹⁸ The list of non-bonded interactions was updated every 10 steps and no cutoff was used. The SHAKE algorithm was used for bonds involving hydrogen atoms and an integration time-step of 2 fs was employed. Internal dielectric constant for the peptide was set to 1, while an external dielectric constant of 80 corresponding to water was employed. All calculations reported in the present work were carried out with the AMBER 9.0 program. Secondary structure analysis was performed using the CLASICO program.¹⁷ The CLASICO program monitors the formation/destruction of secondary structure during the folding process, and characterizes

* To whom correspondence should be addressed. E-mail: bisettyk@dut.ac.za

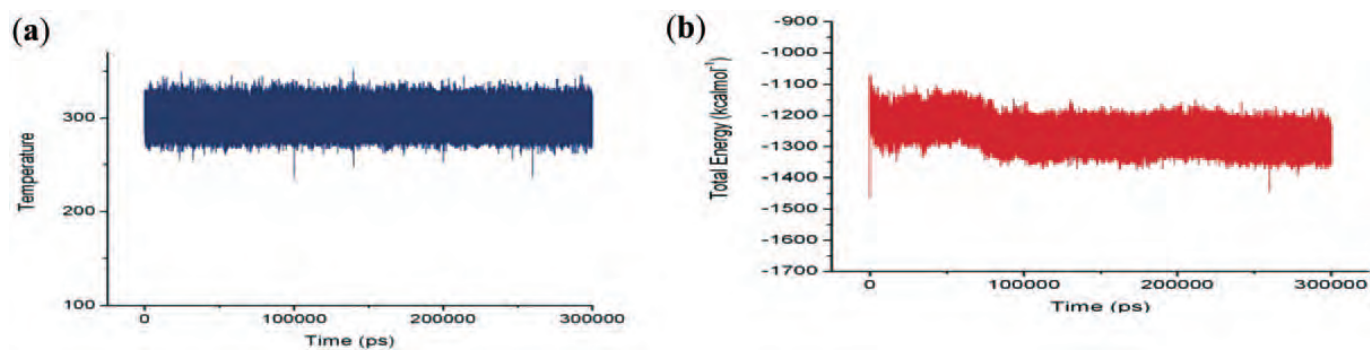


Figure 1 Total energy (a) and Temperature (b) profiles for MD simulation obtained using PTRAJ in AMBER.¹¹

the group of structures that represent the folded molecule. Dihedral angles obtained from the MD trajectory are used as input in this program. The procedure generally involves labeling of the dihedral angles by a string of letters and classification into different conformational patterns by following a two- or three-letter window strings as described by Corcho and co-workers.^{17b,17c} The definition of β -turns used in this study is based on Table 1.

3. Results and Discussion

The thermodynamic parameters such as temperature (Fig. 1a) and the total energy (Fig. 1b) were plotted to measure the quality of the MD trajectory, and clearly reveal that the simulation is relatively stable over the entire MD trajectory. The small decrease in energy (~ 100 Kcal mol⁻¹, Fig. 1b) after ~ 65 ns was probably due to folding of the peptide structure during simulation that remains relatively stable thereafter.

Figure 2 represents the root-mean-square deviations (RMSD) of the MD trajectory monitored relative to the backbone atoms of the starting structure using the PTRAJ module.¹¹ A closer inspection of Fig. 2 reveals significantly higher (1–30 Å) fluctuation from the start of the simulation until 4 ns, clearly indicating larger structural deviations of the sampled conformations compared to the starting structure of lunasin.

However, the extent of fluctuation was significantly reduced (~ 2 Å) from 200 ns onwards for the production run of the MD trajectory. The plateau formed between 200 and 300 ns

segment of the MD trajectory reveals the comparative stability in the structures probably due to their sufficient folding during the MD sampling process. The results also suggest the adequate length of the MD trajectory chosen as the peptide seems to have folded to a considerable extent after 100 ns of the trajectory, and thereafter does not show any sharp changes in the sampled structures.

In order to get a better understanding of the distribution of structures in the MD trajectory, three clusters; cluster I (1–100 ns), cluster II (100–200 ns) and cluster III (200–300 ns), were identified on the basis of their RMSD patterns shown in Fig. 2. The sampling efficiency of each cluster was monitored in terms of their pattern profiles using the CLASICO program, and is pictorially depicted in the Fig. 3a–c. Patterns basically represent the structures classified on the basis of the type of conformational motifs present.^{17b–c} For a batch of 100 000 structures, 96 875 new patterns (Fig. 3a) were observed for cluster I, while 90 000 (Fig. 3b) and 85409 (Fig. 3c) new patterns were obtained for cluster II and cluster III, respectively. The efficiency of these clusters in terms of generating new patterns is in the order: cluster I (96.8 %) > cluster II (90 %) > cluster III (85.4 %). Despite this, cluster III showed maximum similarity of patterns in majority of the conformations, clearly suggesting stability of the simulation in this part of the trajectory which is consistent with the RMSD results obtained in the 200–300 ns segment. Further characterization involved the identification of the secondary structure motifs of the conformations present in

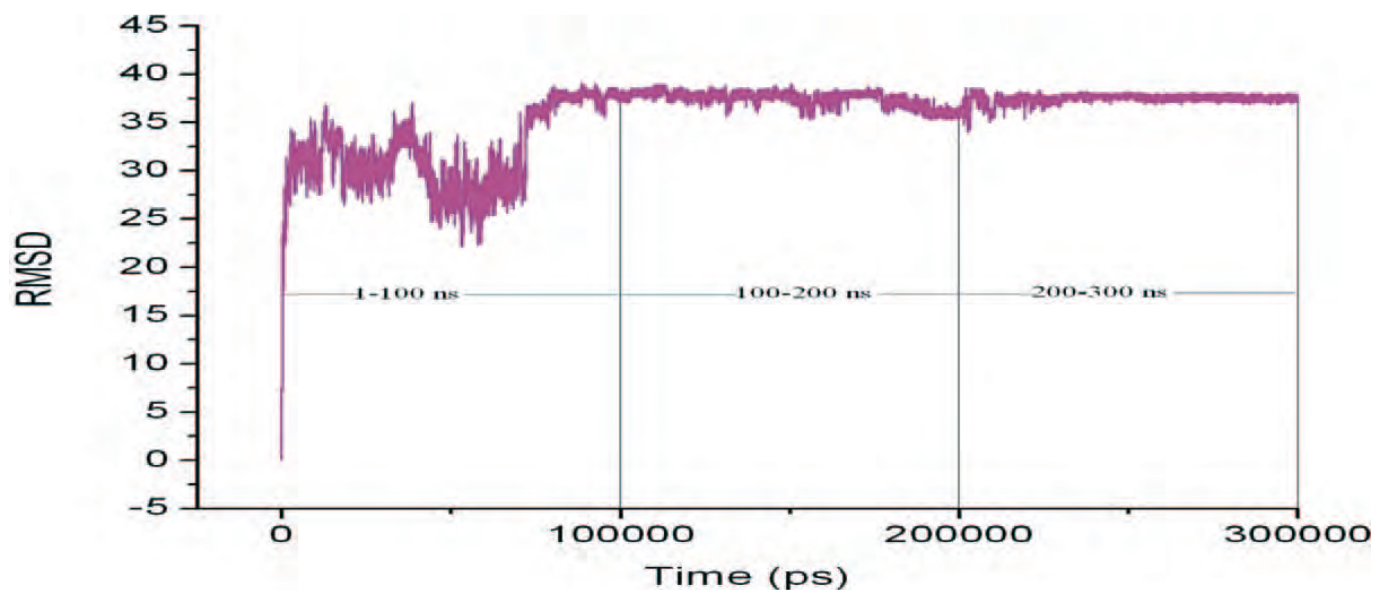


Figure 2 Root mean square deviations (backbone-backbone) of MD trajectory calculated relative to the starting structure. Vertical bars represent the 1–100, 100–200 and 200–300 ns segments of the MD trajectory.

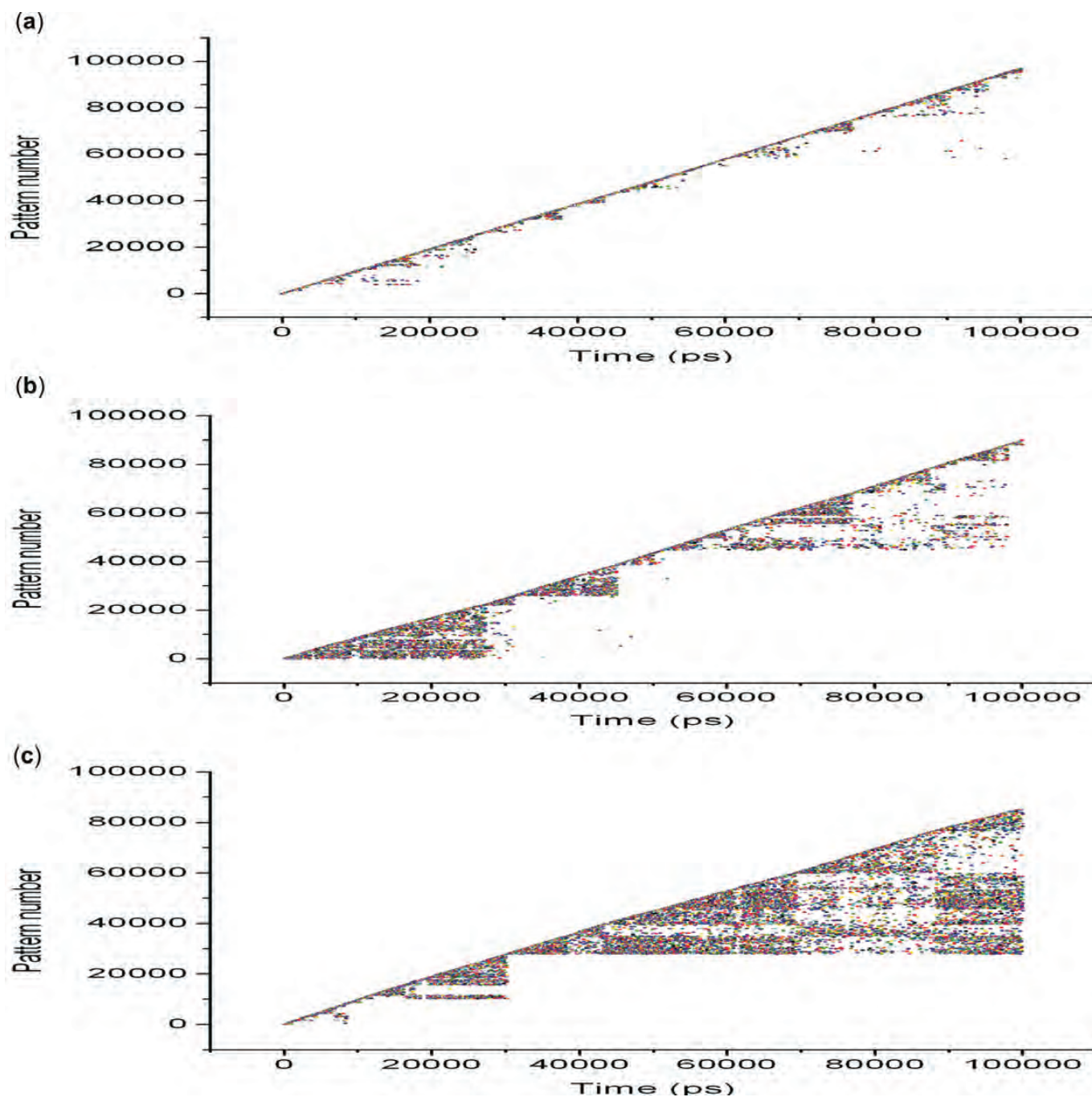


Figure 3 Evolution of patterns along the MD trajectory in the structures of (a) cluster I (b) cluster II and (c) cluster III obtained using the CLASICO program.¹⁷

clusters I–III using the CLASICO program.¹⁷ This program translates each snapshot into a string of letters by computing the backbone dihedral angles for each residue and assigns a letter according to the Zimmerman partition of the Ramachandran map.¹⁹ After considering certain sets of rules, each string is further analyzed using a three-letter window to assign the corresponding secondary motif.

Figure 4a–c represents the statistics of the conformational motifs for each residue of the lunasin peptide in clusters I–III, respectively. A closer inspection of Fig 4a reveals that β -turns are the preferred secondary motifs acquired by most of the residues in the sampled conformations.

To some extent α -helical and 3_{10} α -helical secondary motifs were also observed between residues Trp³-Lys¹², Pro²¹-Lys²⁹ and

Asp³⁸-Asp⁴⁰. Almost similar secondary structure profiles were observed for the clusters II and III as depicted in Fig. 4b and Fig. 4c, respectively.

The β -turn secondary motifs attained by residues of the lunasin peptide were further classified into different types (Table 1) using the two-residue window of the CLASICO program¹⁷, and are pictorially depicted in Fig. 5a–c. Clearly, all residues except Pro²¹, Arg³³-Gly³⁴, exhibited β -turn type I in the conformations of cluster I (Fig. 5a). While residues Gln¹³-Leu¹⁴ and Gly¹⁶-Val¹⁷ adopted β -turn type II and β -turn type ii (mirror image of β -turn type II), respectively, in addition to the β -turn type I observed in cluster I. The conformations sampled in cluster II (Fig. 5b) and cluster III (Fig. 5c) exhibited almost similar profiles showing β -turn type I as their preferred secondary

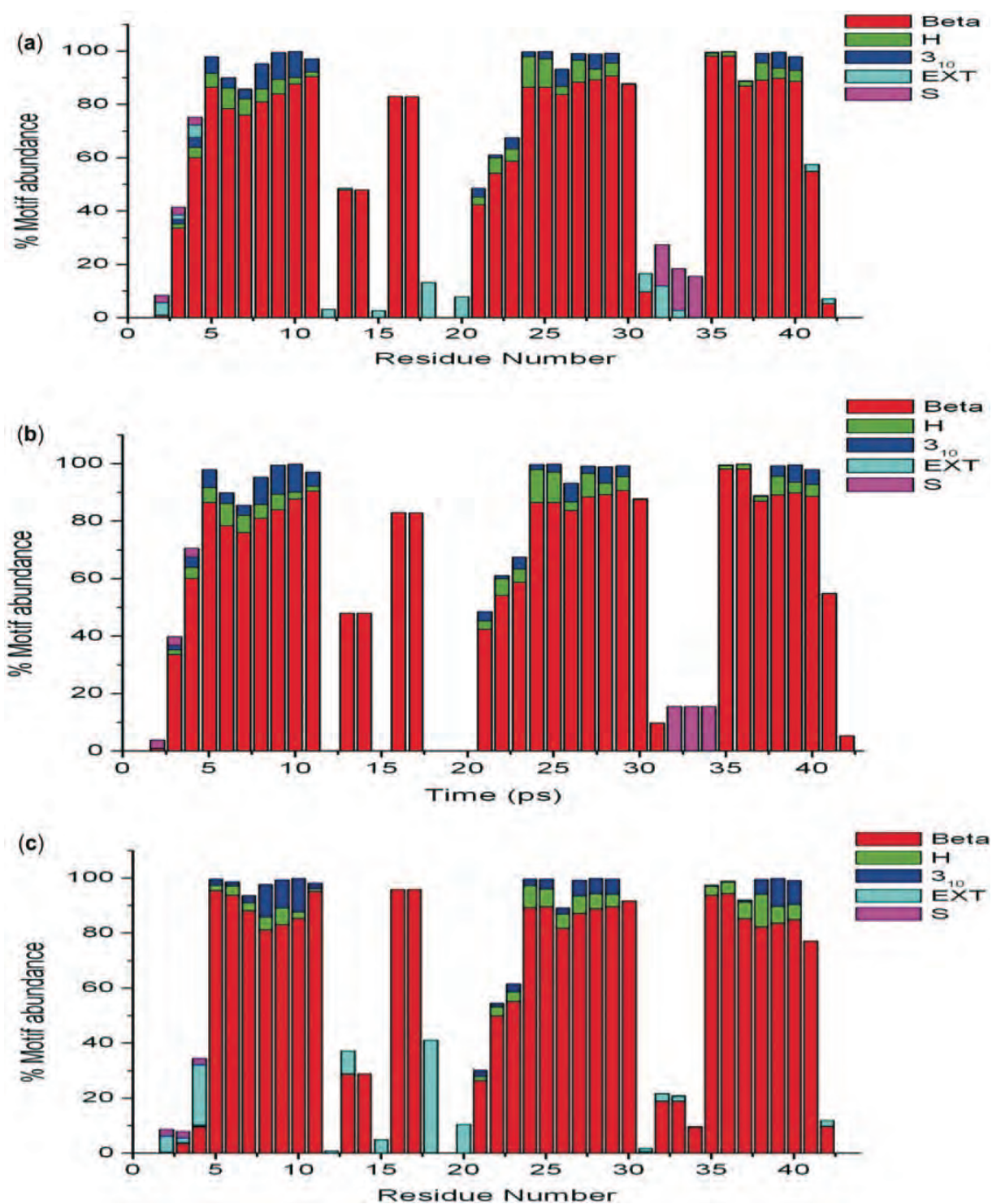


Figure 4 Motif abundance for the lunasin in (a) cluster I, (b) cluster II, and (c) cluster III. Motifs are labelled as: H (α -helix), 3₁₀ (3₁₀-helix), EXT (extended), S (β -strand), Beta (β -turn).¹⁷

feature in both the terminal and some of the central residues. However, the extent of β -turns was more predominant in cluster III relative to cluster II. In both clusters II and III, residues

Table 1 Definition of β -turns based on dihedral angles.^{17b,17c}

Type	$\phi(i+1)$	$\psi(i+1)$	$\phi(i+2)$	$\psi(i+2)$
I	[-110, -10]	[-80, 20]	[-140, -40]	[-50, 50]
II	[-110, -10]	[70, 170]	[30, 130]	[-50, 50]
ii	[110, 10]	[-70, -170]	[-30, -130]	[50, -50]

Gln¹³-Leu¹⁴ adopted β -turn type II, while residues Arg¹¹, Gln¹⁵, Asn¹⁸-Thr²⁰ and Gln³¹ did not show any secondary structure features. Despite having large differences in RMSD values, the secondary structure analysis performed could not efficiently distinguish between the structural features of structures present in clusters I–III. Therefore, the observed propensities of clusters I–III were further rationalized by intramolecular hydrogen bond analysis performed using PTRAJ module of AMBER 9 program, and the results are summarized in Table 2.

The geometrical criterion used for the donor (A)-acceptor (B) distance was ≤ 3.0 Å and the angle HAB ($<HAB$) $\leq 120^\circ$. In

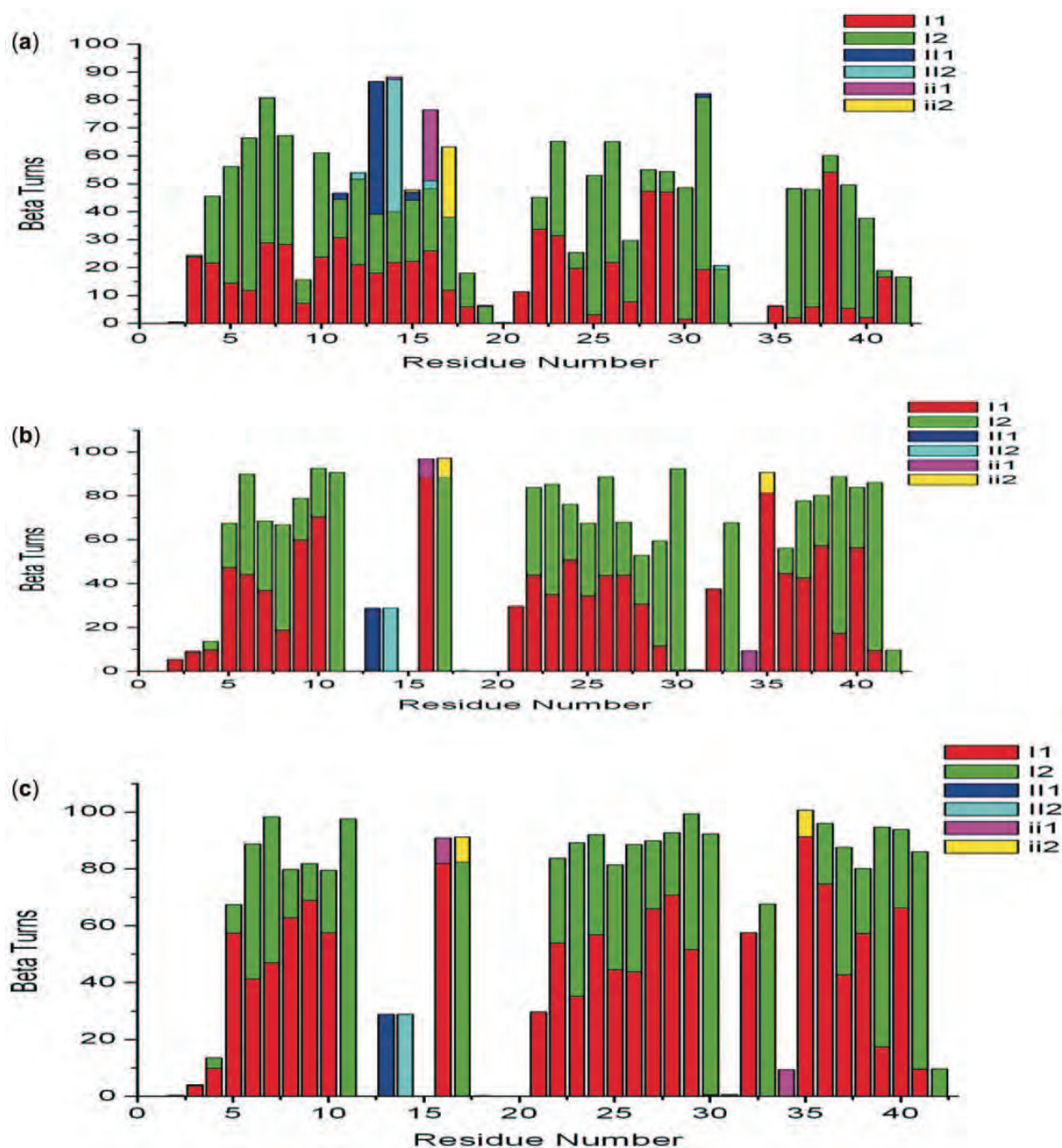


Figure 5 Different types of β -turns attained by the lunasin peptide in (a) cluster I (b) cluster II and (c) cluster III.¹⁷

this case, A is donor (i.e. N-H) and B the acceptor (i.e. O of carbonyl group). Only those hydrogen bonds comprising 1.0 % of the clusters (I, II and III) were considered for analysis. The hydrogen bond between i and $i + 3$ residues correspond to a β -turn, while that between i and $i + 4$ residues represent an α -helical conformation. The results obtained revealed that conformations in cluster I adopted β -turns predominantly in the central residues (Gln¹³-Gln¹⁵, Lys²⁹-Gly³², Gly³⁴-Asp³⁷), and were in agreement with those obtained from the secondary structure analysis described earlier. To some extent the α -helical regions were also seen between residues Gln⁴-Asp⁸, Gln⁷-Arg¹¹, Glu²³-Met²⁷ and Gly³⁴-Asp³⁸ in the structures present in cluster I. The conformations present in clusters II and III on other hand, exhibited predominantly three common α -helical regions in their N-terminus (Trp³-Gln⁷, Gln⁴-Asp⁸, Gln⁷-Arg¹¹), C-terminus

(Met²⁷-Gln³¹, Gly³⁴-Asp³⁸, Asp³⁸-Asp⁴²) and central regions (Pro²¹-His²⁵, Glu²³-Met²⁷, Lys²⁴-Glu²⁸). To some extent β -turns between residues Gln⁴-Gln⁷, Gln⁴-Cys¹⁰ and Asp⁸-Arg¹¹ were also present in cluster III. A characteristic loop formed between residues Cys¹⁰-Cys²² in clusters I and III, but absent in cluster II (Table 2). Hence our results suggests the predominance of the α -helicity in clusters II and III, on the basis of hydrogen bond analysis, were in disagreement with those obtained from the secondary structure analysis, where β -turns were the preferred secondary structure motifs of these clusters. Since, the assignment of helicity in the CLASICO program requires the coexistence of three type I β -turns in the consecutive residues, it is believed that the formation of turns in the residues were not long enough for their coexistence. However, the presence of mixed helices i.e. α - α -3₁₀ and not α - α - α are required for assign-

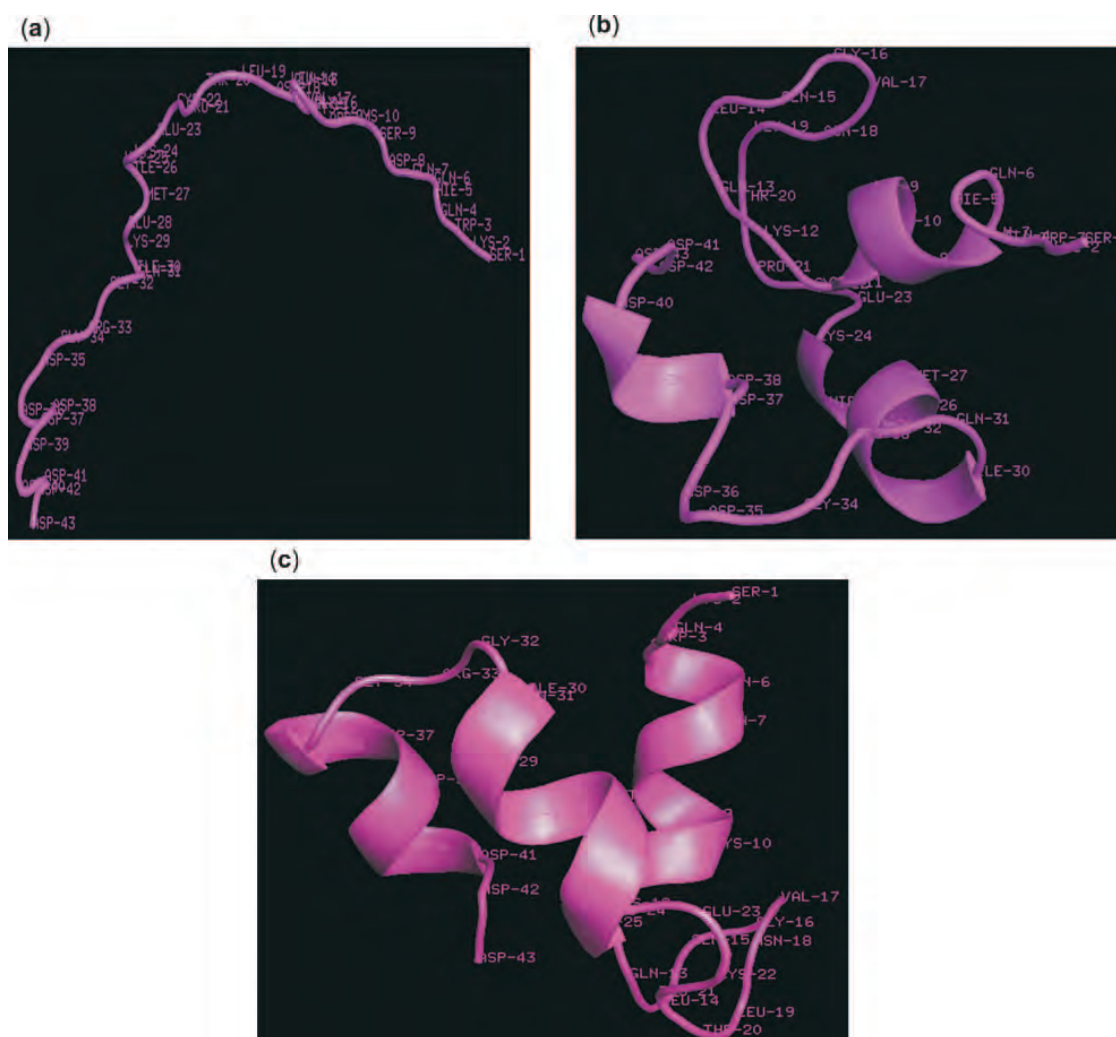


Figure 6 Average structures of the conformations present in (a) cluster I (b) cluster II and (c) cluster III obtained using PTRAJ module of AMBER.

ment of α -helicity), also accounts for the underestimation of α -helices in the CLASICO program.

In order to get a clearer picture of the structural features of clusters I–III, the average structures were obtained for each

Table 2 Secondary structures observed due to backbone-backbone hydrogen bond interactions and their percentages in three main clusters (I, II and III) for Lunasin. Clusters I, II and III refer to 1–100, 100–200 and 200–300 ns segments of the MD trajectory, respectively.

Donor-acceptor	2° structure	Cluster I	Cluster II	Cluster III
(Gln ⁴)O...N(Gln ⁷)	β -turn	22 %	20 %	38 %
(Gln ⁷)O...N(Cys ¹⁰)	β -turn	18 %	–	21 %
(Asp ⁸)O...N(Arg ¹¹)	β -turn	–	–	18 %
(Gln ¹³)O...N(Gln ¹⁵)	β -turn	50 %	–	–
(Lys ²⁹)O...N(Gly ³²)	β -turn	47 %	–	–
(Gly ³⁴)O...N(Asp ³⁷)	β -turn	38 %	18 %	–
(Asp ³⁸)O...N(Asp ⁴¹)	β -turn	–	14 %	–
(Trp ³)O...N(Gln ⁷)	α -helical	–	12 %	33 %
(Gln ⁴)O...N(Asp ⁸)	α -helical	8 %	17 %	24 %
(Gln ⁷)O...N(Arg ¹¹)	α -helical	9 %	45 %	22 %
(Thr ²⁰)O...N(Lys ²⁴)	α -helical	–	25 %	12 %
(Pro ²¹)O...N(His ²⁵)	α -helical	–	44 %	14 %
(Glu ²³)O...N(Met ²⁷)	α -helical	12 %	49 %	52 %
(Lys ²⁴)O...N(Glu ²⁸)	α -helical	–	38 %	24 %
(Met ²⁷)O...N(Gln ³¹)	α -helical	–	58 %	29 %
(Gly ³⁴)O...N(Asp ³⁸)	α -helical	21 %	46 %	44 %
(Asp ³⁸)O...N(Asp ⁴²)	α -helical	–	35 %	22 %
(Cys ¹⁰)O...N(Cys ²²)	Loop	44 %	–	32 %

cluster using PTRAJ, and are diagrammatically represented in Fig. 6a–c, respectively. In the case of cluster I, the average structure showed only turns and loops, clearly supporting the results obtained from secondary structure analysis and hydrogen bond analysis. For cluster II the average structure exhibited three different α -helical regions; one between residues Gln⁷–Arg¹¹, the second between residues Lys²⁴–Ile³⁰ and the third flanked by residues Asp³⁸–Asp⁴⁰. Similarly, cluster III also showed three α -helical regions flanked by residues His⁵–Arg¹¹, His²⁵–Gln³¹ and Asp³⁵–Asp⁴¹ in the N-terminus, C-terminus and central region of peptide, respectively.

The structures sampled in the last 200 ns segment of the MD were further classified on the basis of their structural patterns using Kleiweg's clustering algorithm.²⁰ For this purpose, 5000 structures were chosen as representative structures considering snapshots at 40 p s intervals. Using the RMSD of the coordinates of the backbone atoms between two configurations as a distance, a dendrogram shown pictorially in Fig. 7 was generated employing different Kleiweg's clustering scripts (<http://www.let.rug.nl/kleiweg/clustering/>). The structural details of cluster analysis are summarized in Table 3.

Figure 7 depicts 4 clusters on the basis of the colour scheme. Clearly, there are no gaps observed at the bottom (corresponding to lower cutoff values) of each cluster thus suggesting a greater overlap of structures in that region, in contrast to the top end (corresponding to higher cutoff values). Consequently, a cutoff value of 2.4 units chosen in this study corresponds to

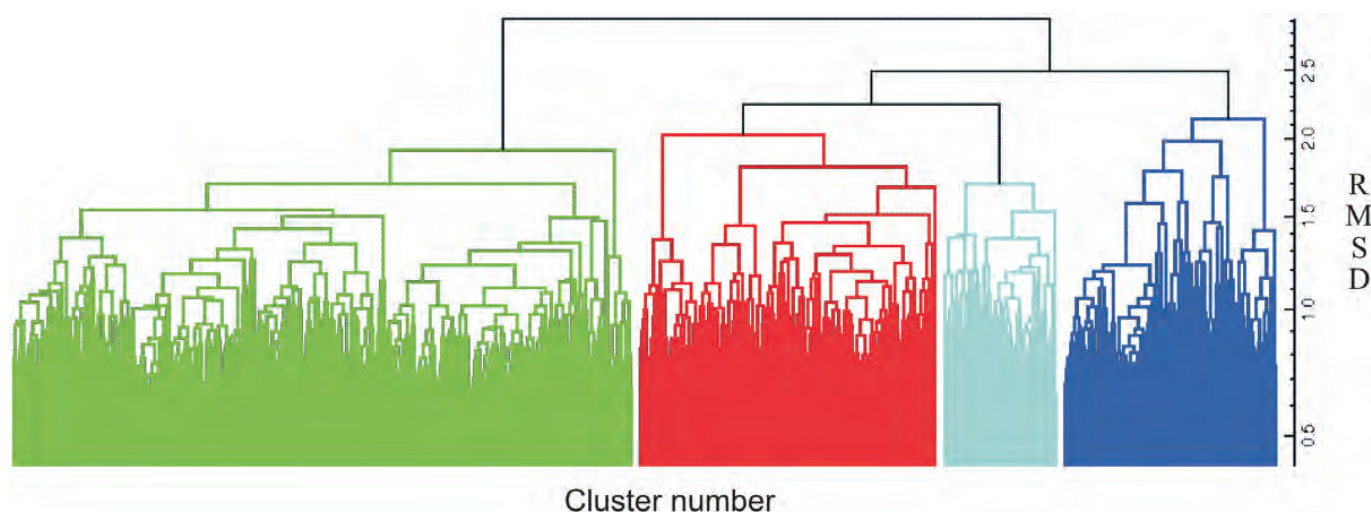


Figure 7 Dendrogram showing different clusters for lunasin classified using the Kleiweg clustering method.²⁰ Different number of clusters can be ascertained by considering different cutoff values of the RMSD across the *y*-axis. Although the colour scheme indicates four clusters, eight clusters (considering a cutoff value of 2.4) have been chosen in this study to observe a greater conformational diversity in the MD.

Table 3 Cluster analysis of lunasin.²⁰

Cluster:	C1	C2	C3	C4	C5	C6	C7	C8
Percentage of structures in cluster	3	2	7	19	4	5	12	48
Major secondary motif of representative structure	β -turn	Extended	α -helical	α -helical	β -turn	Extended	α -helical	α -helical

the formation of eight unique clusters so as to have a greater conformational variety of the MD trajectory. The three most abundant clusters (RMSD cutoff 2.4, Fig. 7) represented by C4, C7 and C8 in Table 3 corresponds to 19 %, 12 % and 48 % of the total number of structures, respectively, clearly suggesting that the bulk of the structures are restricted to small number of clusters. Inspection of Table 3 reveals that 79 % of the structures are represented by the three most abundant clusters (C4, C7, C8) while 21 % acquired by five minor clusters (C1, C2, C3, C5, C6). Moreover, the major secondary motif attained by most of the structures in major clusters was α -helical, while turns or extended form predominated in the minor clusters.

Figure 8 represents the incidence of eight clusters for the 5000 representative structures of the MD. As it can be seen that all the three major clusters (C4, C5, and C7) are acquired by most of the structures ranging between numbers 2500 and 4900. The

most abundant cluster C8 starts growing from the beginning of the MD and keeps adding the structures throughout the sampling process. The lowest number of structures corresponds to clusters C1 and C2.

Of the eight clusters identified (RMSD cutoff 1.9, Fig. 7), three major clusters (C4, C7 and C8) containing the most similar conformations were subjected to the secondary structure analysis using the CLASICO program.¹⁷ Histograms displaying the statistics of different secondary motifs attained by each residue of the peptide in major clusters C4, C7 and C8 are depicted in Fig. 9a–c, respectively. A closer inspection of Fig. 9a reveals that most of the structures in second most populated cluster C4 exhibit predominant β -turn type I between residues Trp³-Arg¹¹, Cys²²-Gln³¹ and Asp³⁵-Asp⁴¹, while the intervening residues (11, 14, 18–21, 32–34) do not show any secondary structure characteristics.

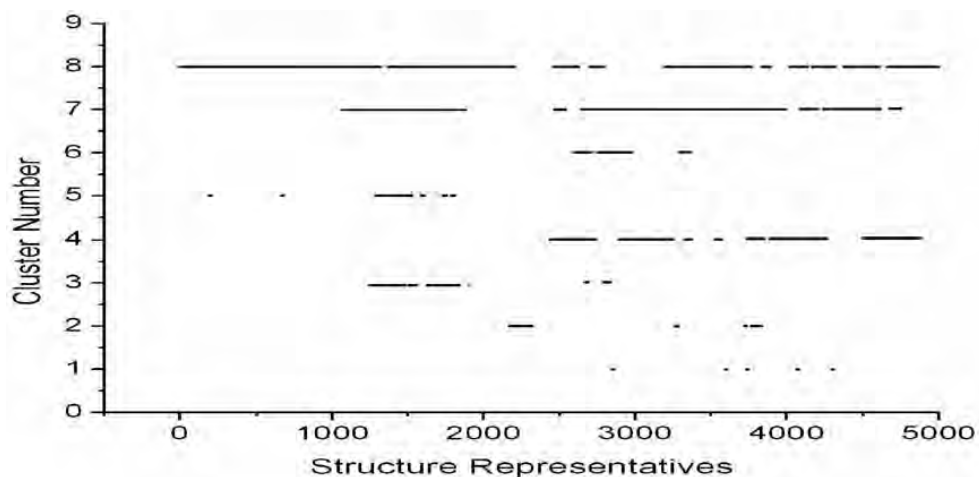


Figure 8 Evolution of eight clusters during the progress of MD for representative structures obtained using Kleiweg clustering method.²⁰ Solid lines in different regions indicate the greater number of closely related structures in the cluster.

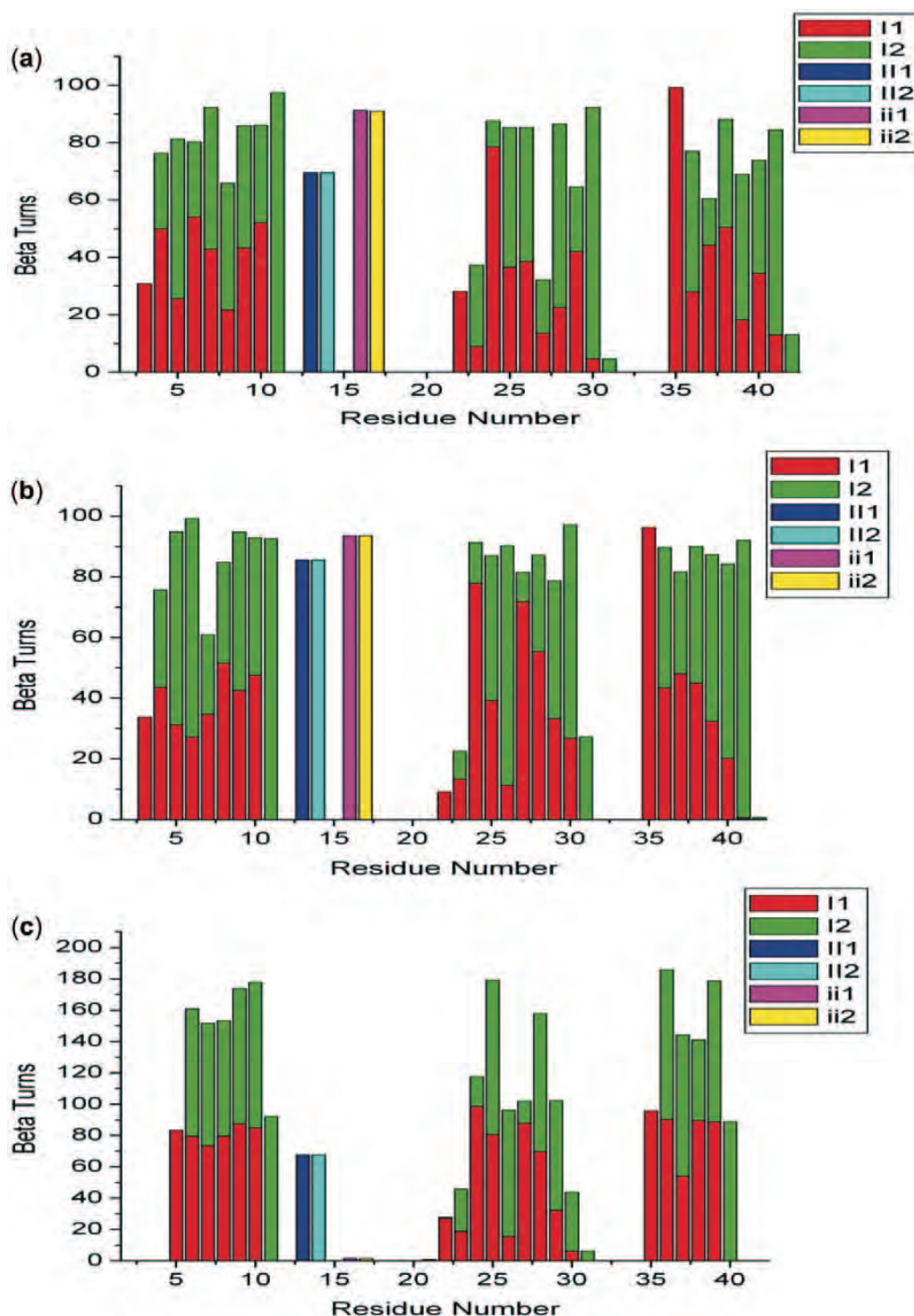


Figure 9 Different types of β -turns attained by the lunasin peptide in three major clusters (a) C4 (b) C7 and (c) C8.¹⁷

The structures of first (C8, Table 2) and third (C7, Table 2) most populated clusters also exhibited almost similar trend, although in different percentages, as that of cluster C4 exhibiting β -turn type I as their preferred secondary motif. To some extent, β -turn type II between residues Gln¹³-Leu¹⁴ was also observed in all major clusters, while its mirror image (β -turn type ii) between residues Gly¹⁶-Val¹⁷ was absent in cluster C8. Finally, the progress of some important interatomic distances accounting for different α -helical regions was monitored for the last 200 ns segment of MD trajectory, and is diagrammatically represented in Figs 10–11. As it is clear from Fig. 10a that the hydrogen bond distance responsible for helical region between residues

Gln⁴-Asp⁸ fluctuates predominantly between 3 and 5 Å throughout this segment of the trajectory. The increased fluctuation (3–9 Å) between residues Gln⁷-Arg¹¹ (Fig. 10b), on other hand, suggests loss of helicity in this part of peptide structure during the sampling process. The helical region flanked by residues Cys²²-Ile²⁶ can be seen in 150 ns of trajectory and sustains for next 75 ns (Fig. 11a), while that between residues Ile²⁶-Ile³⁰ was observed in random structures throughout the sampling process (Fig. 11b).

A closer inspection of Fig. 11c–d reveals that the α -helicity was quite stable in the region flanked by residues Asp³⁵-Asp³⁹ throughout the sampling process, however, a significant loss

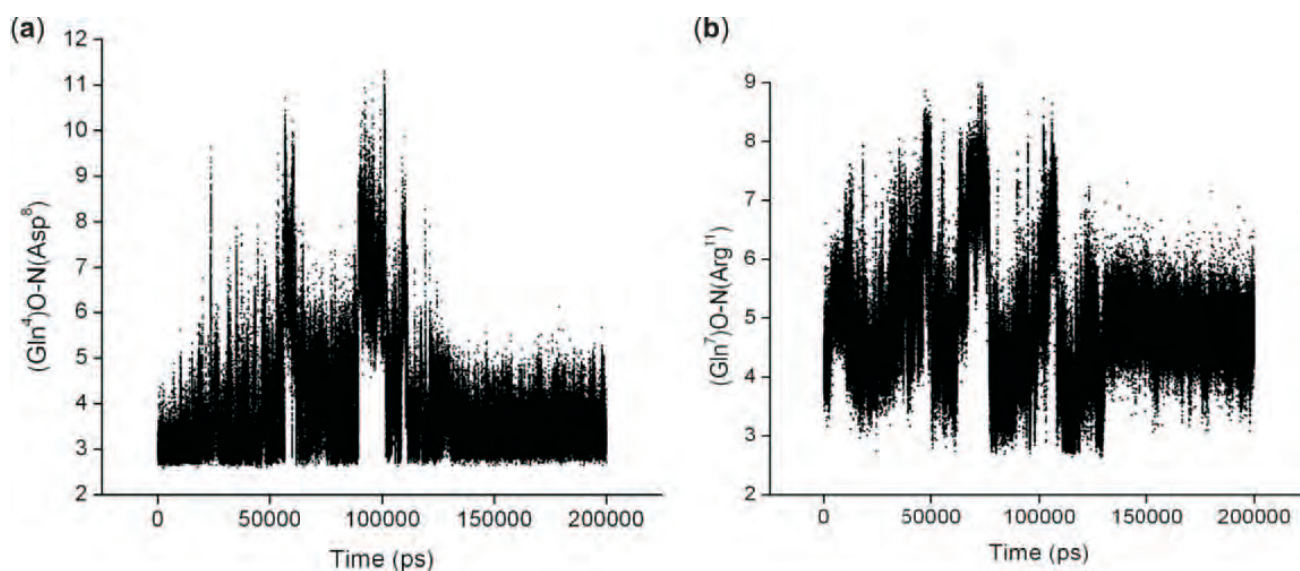


Figure 10 Evolution of distance between residues Gln⁴ and Asp⁸ (a) and Gln⁷ and Arg¹¹ (b) monitored during the 100–300 ns segment of the MD trajectory.

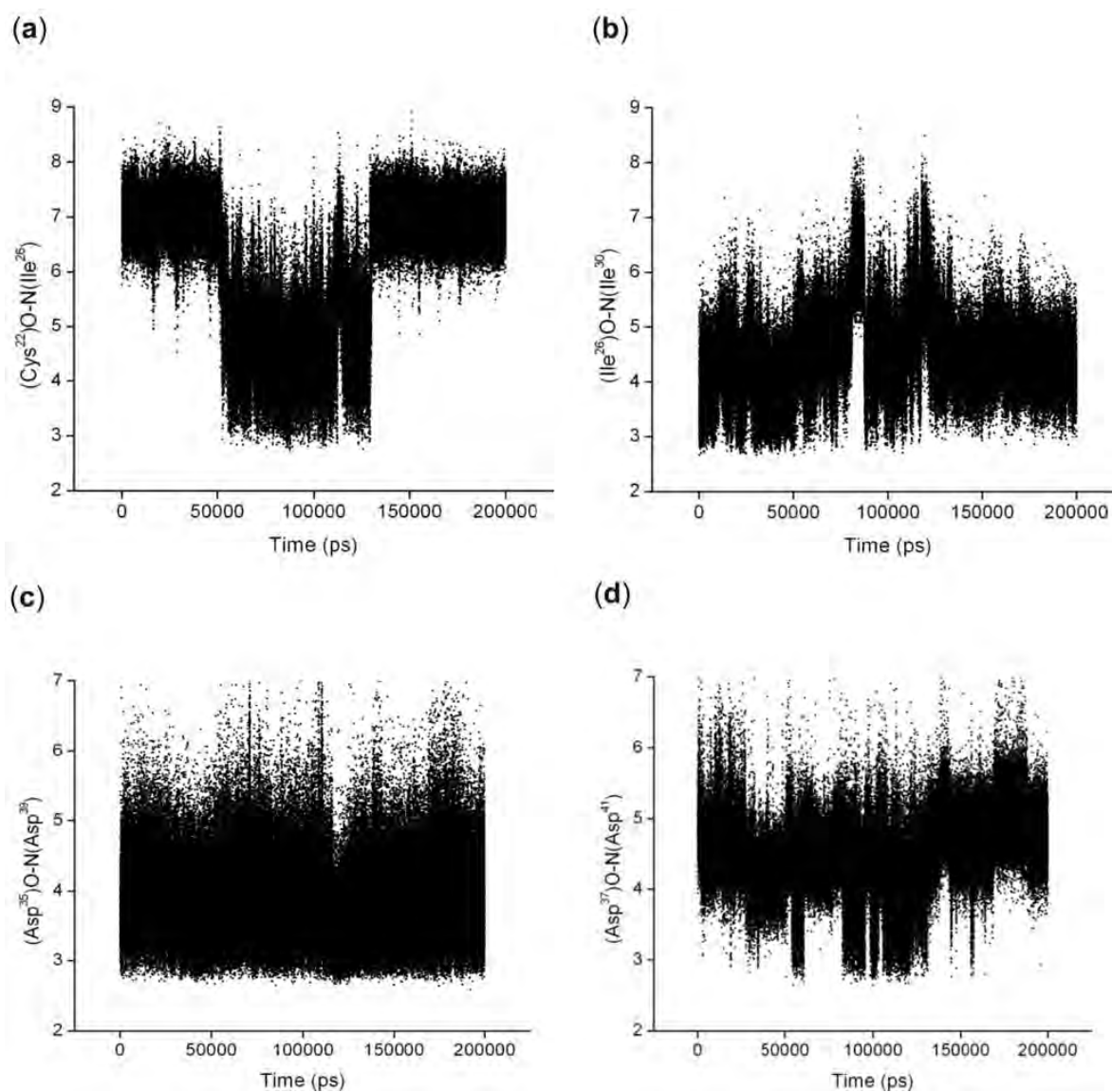


Figure 11 Evolution of distance between residues Cys²² and Ile²⁶ (a), Ile²⁶ and Ile³⁰ (b), Asp³⁵ and Asp³⁹ (c) and Asp³⁷ and Asp⁴¹ (d) monitored during the 100–300 ns segment of the MD trajectory.

was observed in the terminal Asp residues clearly supporting our results based on the secondary structure analysis (Fig. 5).

Overall, these results reveal that lunasin peptide has a stronger propensity to attain three separate α -helical regions flanked by residues His⁵-Cys¹⁰ (N-terminus), Cys²²-Ile³⁰ (central region) and Asp³⁵-Asp⁴¹ (C-terminus) disrupted by few intervening unstructured/extended amino acid residues, and leaving last two C-terminus Asp residues unstructured. Interestingly, the cell adhesion motif of lunasin composed of arginine-glycine-aspartic acid residues (RGD) did not reveal any characteristic secondary features, whereas majority of tail residues (Asp³⁵-Asp⁴¹) adopted a well-defined α -helical region. Accordingly, the dynamical picture emerging is that RGD group probably acts as a hinge, supporting the α -helical region between central residues on the one hand and C-terminal residues on the other. It is believed that the presence of α -helicity in the terminal aspartic acid residues of lunasin could have some significant role in its binding with the chromatin. However, other sampling techniques (REMD and SA) will be used in our future investigations to support the proposed conformation of lunasin and to rule out any possibility of its entrapment at higher potential energy surface in the current MD study.

4. Conclusions

The present study involves the utilization of MD simulations to fully explore the conformational profile of a novel cancer-preventative, 43 residue lunasin peptide, starting from an extended structure. For this purpose, a 300 ns MD simulation was performed using the GB-OBC approximation under implicit solvent conditions. The aggregated information obtained from the analysis indicates that the lunasin peptide adopts three separate α -helical regions in its structure intervened by some unstructured or extended residues. However, the last few residues of both N- and C-terminus remain extended or unstructured. Moreover, the cell adhesion motif (RGD) plays a role of hinge winding and unwinding the central and C-terminus helical regions of the peptide. It is believed that the α -helicity associated with C-terminal aspartic acid residues of lunasin play a recognition role in its binding with the chromatin residue and could thus be responsible for its antimitotic action in the mammalian cell lines. The structural information obtained from the present study could be helpful to better understand the bioactive conformation of lunasin for future investigations, and can be further used in the design of new anti-cancer peptides with similar activity profiles.

Acknowledgements

Dr. P. Singh gratefully acknowledges financial support from the Durban University of Technology and the National Research Foundation for the position of a Research Associate. K.B. grate-

fully acknowledges the experiences and insights gained from the Spanish collaborators (Professor Juan J Perez and co-workers) – through the SA–Spain bilateral agreement. The authors would like to express their acknowledgement to the Centre for High Performance Computing, an initiative supported by the Department of Science and Technology of South Africa.

References

- 1 A.F. Galvez, M.J.R. Revilla and B.O. de Lumen, *Plant Physiol.*, 1997, **114**, 1567–1569.
- 2 B. Hernandez-Ledesma, C. Hsieh and B.O. de Lumen. *Peptides*, 2009, **30**, 426–430.
- 3 V.P. Dia, W. Wang, V.L. Oh, B.O. de Lumen and E. Gonzalez de Mejia, *Food Chem.*, 2009, **114**, 108–115.
- 4 H.J. Jeong, J.B. Jeong, D.S. Kim, J.H. Park, J.B. Lee and D.H. Kweon, *Cancer Lett.* 2007, **255**, 42–48.
- 5 A.F. Galvez, N. Chen, J. Macasieb and B.O. de Lumen, *Cancer Res.*, 2001, **61**, 7473–7478.
- 6 J.H. Jeong, J.H. Park, Y. Lam and B.O. de Lumen, *J. Agric. Food Chem.* 2003, **51**, 7901–7906.
- 7 E. Hsieh, C.M. Chai and B.O. de Lumen, *J. Invest. Dermatol.*, 2004, **123**, 530–536.
- 8 E.G. de Mejia and V.P. Dia, *Peptides*, 2009, **30**, 2388–2398.
- 9 H.J. Jeong, J.B. Jeong, D.S. Kim and B.O. de Lumen, *J. Agric. Food Chem.*, 2007, **55**, 632–637.
- 10 J.H. Park, H.J. Jeong and B.O. de Lumen, *J. Agric. Food Chem.*, 2007, **55**, 10703–10706.
- 11 D.A. Case, T.A. Darden, T.E. Cheatham III, C.L. Simmerling, J. Wang, R.E. Duke, R. Luo, K.M. Merz, D.A. Pearlman, M. Crowley, R.C. Walker, W. Zhang, B. Wang, S. Hayik, A. Roitberg, G. Seabra, K.F. Wong, F. Paesani, X. Wu, S. Brozell, V. Tsui, H. Gohlke, L. Yang, C. Tan, J. Mongan, V. Hornak, G. Cui, P. Beroza, D.H. Mathews, C. Schafmeister, W.S. Ross and P.A. Kollman, *AMBER 9*, University of California, San Francisco, 2006.
- 12 P. Singh, P. Sharma, K. Bisetty, F.J. Corcho and J.J. Perez, *Comp. Theor. Chem.*, 2011, **974**, 122–132.
- 13 P. Sharma, P. Singh, K. Bisetty and J.J. Perez, *Comp. Theor. Chem.*, 2011, **971**, 1–7.
- 14 P. Sharma, P. Singh, K. Bisetty, A. Rodriguez and J.J. Perez, *J. Peptide Sci.*, 2011, **17**, 174–183.
- 15 A. Onufriev, D. Bashford, and D.A. Case, *Proteins: Struct. Funct. Bioinf.*, 2004, **55**, 383–394.
- 16 P.A. Kollman, R. Dixon, W. Cornell, T. Fox, C. Chipot and A. Pohorille, *Comp. Simul. Biomol. Systems* 1997, **3**, 83–96.
- 17 (a) LaFargaCPL: CLASTERIT: Project Info. Available from: <http://devel.cpl.upc.edu/clasterit> (b) F. Corcho, J. Canto and J.J. Perez, *J. Comp. Chem.* 2004, **25**, 1937–1952. (c) F. Corcho, P. Mokoena, K. Bisetty and J.J. Perez, *Biopolymers*, 2009, **91**, 391–400.
- 18 R.W. Pastor, B.R. Brooks and A. Szabo, *Mol. Phys.* 1988, **65**, 1409–1419.
- 19 S.S. Zimmerman, M.S. Pottle, G. Nemethy and H.A. Scheraga, *Macromol.*, 1977, **10**, 1–9.
- 20 P. Kleiweg, J. Nerbonne and L. Bosveld, in *Diagrammatic Representation and Inference*. 3rd Intn'l Conf., Diagrams 2004. Cambridge, UK. (A. Blackwell, K. Marriott and A. Shimojima, eds.), (Lecture Notes in Artificial Intelligence 2980). Springer, Berlin, 2004, pp. 392–394.